INTERNATIONAL JOURNAL OF OPTIMIZATION IN CIVIL ENGINEERING
Int. J. Optim. Civil Eng., 2025; 15(2):221-240

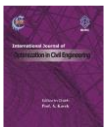

OPTIMIZATION OF THE PARAMETERS OF THE TRIPLE FRICTION PENDULUM BEARING SYSTEMS FOR A THREE-DIMENSIONAL FRAME WITH NONLINEAR BEHAVIOUR

R. Kamgar[*, †], A. Ahmadi, and A. Ghale Sefidi
Department of Civil Engineering, Shahrekord University, Shahrekord, Iran

ABSTRACT

This paper utilized the multi-objective cuckoo search (mocs) optimization algorithm to compute the optimum parameters of three-dimensional frame structures controlled by the triple friction pendulum bearing (TFPB) systems. For this purpose, firstly, the maximum capacity of the unisolated structure (uncontrolled structures) is evaluated for six main earthquakes using an incremental dynamic analysis (IDA). Then, the structure is controlled using the TFPB systems and excited using the maximum acceleration calculated from the previous step to calculate the optimal parameters of the TFPB system (i.e., the coefficients of friction and effective radius of curvature) subjected to some constraints in such a way that the maximum local drift ratio and also the Park-Ang damage index ratio minimized. Finally, to evaluate the behavior of the controlled structure, it is excited by main shock-aftershock earthquakes under sequence IDA. The results showed an average seismic improvement of 30% and 40% for the controlled structures according to the Park-Ang damage and drift indices, respectively.

Keywords: Triple friction pendulum bearings, Moment frame, Park-ang damage index, Optimization, Drift ratio.

Received: 23 March 2025; Accepted: 25 May 2025

1. INTRODUCTION

Earthquakes are natural events that are still unpredictable. After years of research and advancement of science and technology, humanity still has not found a pragmatic approach to predict them. The risk of earthquakes has always existed everywhere. This risk may decrease or increase depending on the geological history of the areas and their seismicity.

[*]Corresponding author: Department of Civil Engineering, Shahrekord University, Shahrekord, Iran
[†]E-mail address: kamgar@sku.ac.ir (R. Kamgar)

Many people die or become homeless yearly due to earthquakes in large and densely populated and small and sparsely populated cities. After an earthquake, much damage is inflicted on societies, most irreparable. Therefore, although earthquakes are unpredictable, myriad research has been done on reducing these damages, and some reliable measures have been developed to reduce these damages [1-2].

Structures, one of the most important parts of human societies, must properly perform to save lives during an earthquake. Therefore, the proper design and implementation are of paramount importance. In recent years, the philosophy of the codes has shifted toward designing flexible buildings to dissipate seismic energy as much as possible. With the progress of science and technology, many methods have been invented for reducing earthquake damage, including strengthening and vibration control systems. Among mentioned methods, vibration control systems have attracted the attention of researchers as they have different benefits from a practical point of view.

An essential parameter in the structure elastic design procedure is the base shear, which is the accumulated lateral force applied to structures. However, in a severe earthquake, the base shear may exceed the shear elastic capacity of the structure; therefore, its behavior would be nonlinear, and structures have a higher capacity due to overlooked plastic behavior and energy absorption capacity.

The damage index is another parameter that can be used to evaluate the damage status of a structure. This index considers various parameters such as absorbed energy in members, members' displacement, stories' drift, and ductility of structural members, representing a quantitive perspective of the damage inflicted on the structure [1]. Several failure indicators have been introduced by researchers so far. They interpreted structural failure based on either members' deformation or energy dissipation [2]. Another failure indicator built upon the previous two criteria, among which the Park-Ang damage index is the most prominent. In this type, the failure index is calculated based on the linear combination of the sum of the maximum ductility and energy dissipated by the members [3]. The former category develops damage indicators based on changes in some specific dynamic characteristics of structures (e.g., Ghobarah et al. [4]).

Furthermore, there are some hybrid methods concurrently employing quantitative and qualitative indices. Quantitative methods rectify the usually overestimated structural damage of qualitative methods, and a unique number represents the damage status of the entire structure [5]. An effort to find the consistency of these indices was made by Estekanchi et al. [6]. They investigated damage indices based on dissipated energy, modal parameters, deformation, and cyclic fatigue behavior to detect their correlation. They displayed the correlation between them graphically and provided approximate formulas to convert them to each other. Nowadays, the Park-Ang Damage index has gained momentum and grabbed the attention of several researchers because it is accurate and straightforward to use (e.g., Khaaloo and Omidi [7] and Behnamfar et al. [8]). For the same reasons, we also employed the Park-Ang damage index as a suitable tool to calculate the damage index of elements, stories, and structures.

One of the appropriate technologies to improve the structure's performance in low-rise structures is installing isolators on column bases. Friction pendulum isolators are of these separators, first introduced by Zayas and Mahin [9]. The earliest generation of these separators was a single friction pendulum bearing, consisting of a concave plate with a

sphere in its middle, lubricated with a specific material. As time went by, double, triple, and quintuple friction pendulum bearings were developed based on the required capacity. These isolators transfer the movement between different slides, and by doing so, they change the stiffness and damping of structures [10]. For the first time, Zayas et al. (1987) and then Mokha et al. (1990) modeled and described the single friction pendulum bearing (SFPB), which is considered the simplest type of separator with one stage of operation [11]. After that, Fenz and Constantinou [10] presented a double friction pendulum bearing advantages such as reducing heating effects and increasing displacement capacity. In the following, several researchers studied the behavior, modeling, and design of multiple friction pendulum bearings. Fenz and Constantinou [12], in a comprehensive study, described the behavior of this type of separator in detail. He also presented a model of double and triple separators in another paper in 2008, which became the basis of many subsequent types of research on double and triple separators [10]. Later, shaking table experiments and actual modeling was performed on these separators, which immensely helped to understand the behavior of these separators [13]. In other studies, Keikha and Ghodrati Amiri [14] investigated the effect of velocity and temperature on choosing the lubricating materials used in these separators.

Recently, the application of optimization algorithms (e.g., Refs. [15-16]) to improve the seismic performance of structures has proliferated. In an attempt, Medarami et al. (2020) employed the multi-objective cuckoo search (CS) optimization algorithm to reduce the displacement of the base and the acceleration of the roof by optimizing pure friction isolators. Results show that pure friction systems have acceptable performance in reducing seismic responses, maximum input energy, and structural damage. Moreover, equipping the pure friction isolation system with an optimal recovery device can increase the response of the structure under vibration [17].

As mentioned, no research has been conducted on using TFPB to reduce the Park-Ang damage index for low-rise structures. Most existing research on optimizing the control system has considered displacement, acceleration, and drift stories for single- or multi-objective functions. In this study, the objective function is considered the Park-Ang damage index and drift ratio of stories. Considering that the damage index of Park-Ang is a linear combination of the energy absorbed and the deformation of the structural elements, reducing the damage index leads to a reduction in these values. In this study, the three-dimensional structure is also used in the analysis. For the time history analysis, the IDA and sequence IDA have been used to calculate the capacity of the controlled and uncontrolled structures. Here, the efficiency of the meta-heuristic optimization algorithm (i.e., multi-objective CS) in optimizing TFPB parameters for minimizing the Park-Ang damage index and the maximum drift story of a structure under the main shock earthquake is investigated. Then, under main and aftershock ground motions, this structural performance is analyzed by sequential IDA in terms of the Park-Ang damage index and local and global maximum local drift ratio.

2. TRIPLE FRICTION PENDULUM BEARING

Fenz and Constantinou introduced the triple friction pendulum bearing (TFPB) in 2008. This isolator consists of four concave surfaces with different radii and a central rigid core (see Fig. 1). They can change the stiffness and damping of structures under five regimes with

nonlinear performance (see Fig. 1). This isolator comprises a series of steel sliders with specific curvature radius placed on top of each other and a rigid steel core located in their center. The movement of the structure slides these sliders on each other [14]. Three parameters determine the performance of each TFPB: the distance between the two surfaces, d_i, the friction coefficient between the two surfaces μ_i, and the effective radius of each surface. The former parameter can be calculated as Eq. (1).

$$R_{eff} = R_i - h_i \tag{1}$$

where R_{eff} is the effective radius, R_i is the radius of curvature of the ith surface, and h_i represents the distance between the center of the separator to the story of the i^{th} level.

In the first regime, the central rigid core slides between the two inner surfaces when the isolator moves under excitation. In the second regime, the lowest outer surface and the upper inner surface slide. In the third regime, the outermost and upper inner surfaces slide. Finally, the fourth and fifth regimes occur when the upper and lower levels hit the limiting supports. The effective period (T_{eff}) and the equivalent viscous damping (β_{eff}) in each regime can be computed based on the normalized vertical force (*FD*), displacement (*D*), and energy dissipated (*EDC*) in each regime. The dissipated energy is equal to the area of the hysteresis diagram at the same regime [18] (Eqs. 2–4).

$$K_{eff} = \frac{F_D}{D} \tag{2}$$

$$\beta_{eff} = \frac{EDC}{2\pi K_{eff} D^2} \tag{3}$$

$$T_{eff} = 2\pi \sqrt{\frac{1}{gK_{eff}}} \tag{4}$$

where g and K_{eff} show the acceleration of the earth's gravity and the effective stiffness of the TFPB, respectively [14]. The TFPB was coded for the first time by Dao *et al.* [19] in OpenSees®.

3. MODIFIED PARK-ANG DAMAGE INDEX

Park and Ang (1985) introduced this index to quantify structural damage [3]. This index consists of the sum of two parts, the first part is the element's ductility, and the second part is the energy absorption in the element (Eq. 4). Eq. 4 was later modified by Kunnath *et al.* [20] as Eq. (5) [20].

$$DI_{pa} = \frac{\delta_m}{\delta_u} + \beta_{pa} \frac{\int dE}{Q_y \delta_u} \tag{4}$$

$$DI_{Ku} = \frac{\delta_m - \delta_y}{\delta_m - \delta_y} + \beta_{ku} \frac{\int dE}{M_y \theta_u} \tag{5}$$

$$SDI_j = \sum_{k=1}^{m_j} \lambda_{kj} . DI_{kj} \tag{6}$$

$$\lambda_{kj} = \frac{E_{kj}}{\sum_{i=1}^{m_j} E_{ij}} \tag{7}$$

where β_{pa} is a material-dependent coefficient that is between -0.3 and 1.2 for steel structures based on Cosenza *et al.* [21]. However, in this study, we assumed this value is equal to 0.025 based on Refs. [22]. Moreover, δm is the maximum displacement, δ_y is the yielding displacement, δ_u is the final displacement, *dE* is the energy absorption in the element during seismic loading, and M_y is the yielding moment. In addition, *SDIj* is the failure index of the j^{th} story, *DIkj* is the failure index of the k^{th} element from the j^{th} story, and *Ekj* is the hysteretic energy of the k^{th} element from the j^{th} story. Also, Table 1 shows the status of the structural elements based on the Park-Ang damage index value.

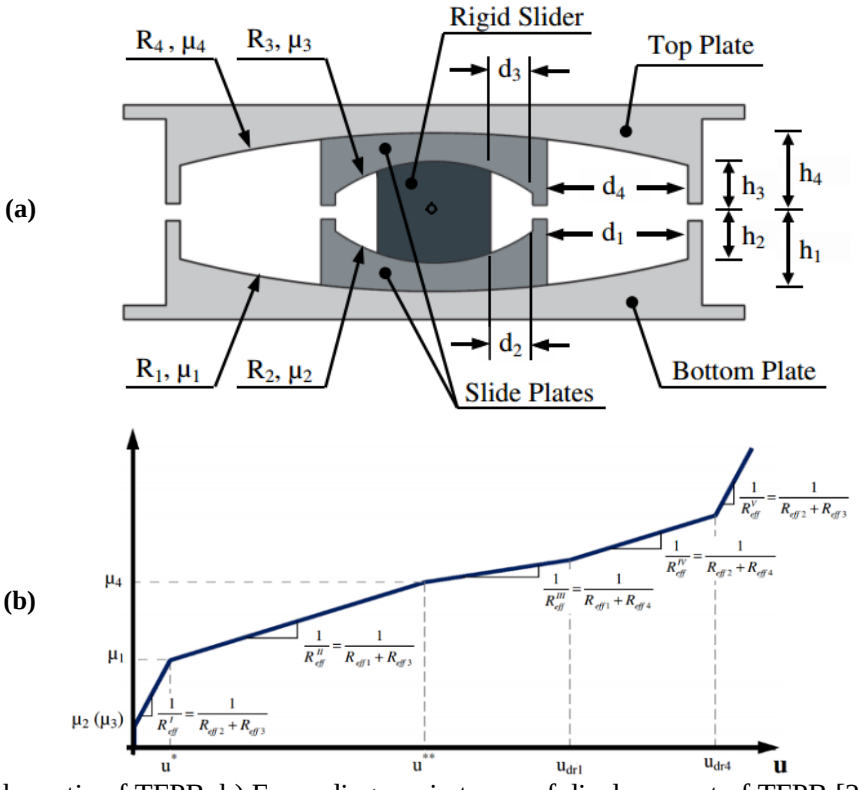

Figure 1: a) A schematic of TFPB, b) Force diagram in terms of displacement of TFPB [23]

Table 1: The damage range of Park-Ang [24].

Damage level	Damage Index	State of Building
Slight	DI< 0.1	No damage
Minor	0.1<DI < 0.25	Minor damage
Moderate	0.25 < DI <0.4	Repairable
Severe	0.4 < DI < 1	Demolition
Collapse	DI<1.0	Loss of Building

4. MULTI-OBJECTIVE CUCKOO SEARCH (MOCS) OPTIMIZATION ALGORITHM

During the last decades, several methods have been proposed for the optimization of structures and the performance of structural components. One of these methods is the MOCS, which is used to solve nonlinear problems. This algorithm, which was first introduced by Yang and Deb (2010) [25], was further investigated by Rajabioun [26]. Salimi *et al.* [27] have also recently employed the MOCS to optimize friction-tuned and tuned mass damper parameters.

In MOCS, the parameters are *n, pa, α*, and *β*, which show the population size, replacement probability, step size, and Lévy flights exponent, respectively. Also, parameters α and β are equal to 0.1 and 1.5, respectively, and parameters *pa* and *n* are considered variables. Notably, the probability of replacement is responsible for creating a balance between local and global optimization.

This algorithm has a series of steps that are expressed as follows for an optimization problem with a *K* target [25]:

If each cuckoo lays *K* eggs at each oviposition and places the eggs in a randomly chosen nest, for each nest *K*, there are solutions, and these solutions are obtained from the following equation:

$$x_i^{t+1} = x_i^t + \alpha \oplus Levy\,(\beta) \tag{8}$$

Eq. (8) $\oplus$ indicates entry-wise multiplications, β also indicates the Lévy flights exponent, and the formula for calculating the parameter α, which suggests the step size, is as follows:

$$\alpha = \alpha_0 \oplus (x_j^t - x_i^t) \tag{9}$$

where x_j^t and x_i^t are two different solutions randomly chosen, the Lévy flights exponent is used to obtain the step size.

Yang and Deb [25] also describe a simpler scheme:

$$s = \alpha_0 \oplus (x_j^t - x_i^t) \oplus Levy\,(\beta) = 0.01(x_j^t - x_i^t)\frac{u}{|v|^{\frac{1}{\beta}}} \tag{10}$$

where *u* and *v* are represented by normal distributions as follows:

$$u \sim N(0,\sigma_u^2), v \sim N(0,\sigma_v^2) \tag{11}$$

Moreover, σ_u and σ_v are defined by the following equation:

$$\begin{aligned} \sigma_u &= \{\frac{G(1+\beta)\sin(\pi\beta/2)}{G[(1+\beta)/2]\beta 2^{(\beta-1)/2}}\}^{1/\beta} \\ \sigma_v &= 1 \end{aligned} \tag{12}$$

Concerning σ_u, G are standard gamma functions that help increase the convergence speed of the cuckoo algorithm. Finally, Eq. 13 generates a new simple random walk solution.

$$x_i^{t+1} = x_i^t + \alpha_0 \oplus H(p_a - \varepsilon) \oplus (x_j^t - x_k^t) \tag{13}$$

H represents the Heaviside function, and α_0 and ε are the step size scaling factor and a random number with a uniform distribution, respectively [25].

5. DEFINITION OF OPTIMIZATION PROBLEM AND CONSTRAINTS

In the present problem, to define the optimization problem, the following constraints are applied to solve the problem.

$$\begin{aligned} &Find \quad R_{eff\ 1,4},\ R_{eff\ 2,3},\ \mu_1, \mu_{2,3}, \mu_4 \\ &minimize: \begin{cases} \dfrac{PADI_{Controled\ \text{structure}}}{PADI_{Uncontroled\ \text{structure}}} \\ \dfrac{maximum\ \ Loacl\ \ Drift^{\,j}{}_{Controled\ \text{structure}}}{maximum\ \ Loacl\ \ Drift^{\,j}{}_{Uncontroled\ \text{structure}}} \end{cases} \\ &Subjected\ \text{to:} \begin{cases} R_{eff_1} = R_{eff_4} >> R_{eff_2} = R_{eff_3} \\ \mu_2 = \mu_3 < \mu_1 < \mu_4 \\ d_1 > (\mu_4 - \mu 1) R_{eff_1} \\ d_2 > (\mu_1 - \mu_2) R_{eff_2} \\ d_3 > (\mu_4 - \mu_3) R_{eff_3} \end{cases} \end{aligned} \tag{14}$$

where μ and R_{eff} are the coefficients of friction and effective radius of curvature for different levels, respectively. Moreover, PADI is the damage index.

6. MODELING AND VALIDATION OF THE STRUCTURE

The studied structure in this research is a 4-story 3D nonlinear steel moment frame with three 5-meter bays in each direction while the height of each story is 3.2 meters. The dead loads of the stories and roof are 550 kg/m^2 and 450 kg/m^2, correspondingly. The live loads of the story and roof are 200 kg/m^2 and 150 kg/m^2, respectively. Loads of the surrounding walls in the stories and roof are 600 *kg/m* and 240 *kg/m*, respectively. The period of the structure without an isolator is equal to 1.16 sec in each direction, and its damping ratio is equal to 0.05. The columns of this structure in the first two and other stories are made of 22 × 1.5 and 18×1.5 boxes, respectively.

The beams in the first to fourth stories are designed as IPE 300, IPE 270, IPE 270, and IPE 220, respectively. This structure is modeled in OpenSees software, which has been used to model the beam and its columns from the ElasticBeamColumn element, which is connected to the zero-length elements that act as bending springs to obtain the nonlinear behavior. These springs operate from the cyclic response based on the modified degenerate bilinear model of Ibarra and Krawinkler [28]. The Triple Friction Pendulum element command models the triple friction pendulum bearing (TFPB). To verify the accuracy of the results, this structure was modeled in ETABS® software as well. The results of Table 2 show that the modeling of the structure has been done with very high accuracy.

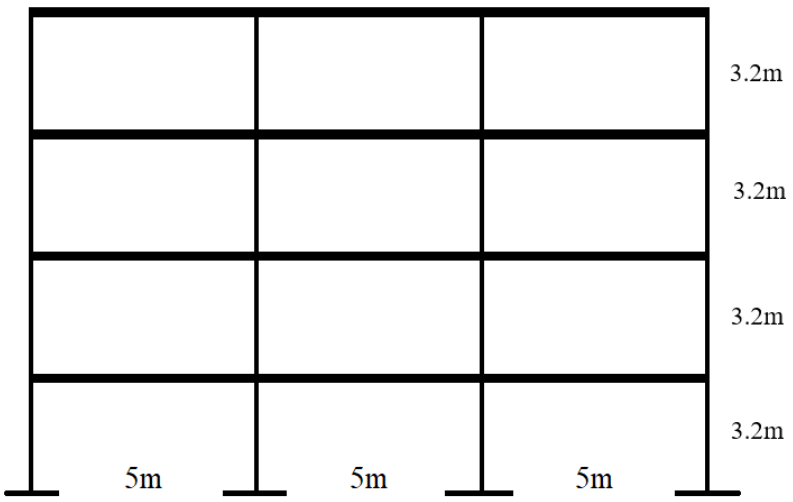

Figure 2: Schematic of the frame of the studied three-dimensional structure (the structure is symmetrical in both directions)

Table 2: Comparison of the cycle time of the structure modeled in OpenSees and the structure modeled in ETABS®

Period	In OpenSees® *(sec)*	In ETABS® *(sec)*
	1.16	1.16

In this study, to verify the modeling of the TFPB, the paper of Fenz and Constantinou [12] is considered. To this end, a three-dimensional shear frame (Fig. 2) with a single degree of freedom, one story, and one opening in each direction is used (Tables 3-4) [12]. In Fenz and Constantinou's research, this structure was modeled in SAP2000® software, while it is modeled in OpenSees® software here. This period damping ratio of structure without any isolator in both directions equals 0.5 sec and 2%, respectively. This structure underwent the earthquake acceleration map of El Centro Arrey #9, multiplied by a factor of 2.15 in the earthquake acceleration values. The nonlinear time history dynamic analysis has been performed. The results show (Fig. 3) that the modeling has a good accuracy compared to Ref. [23].

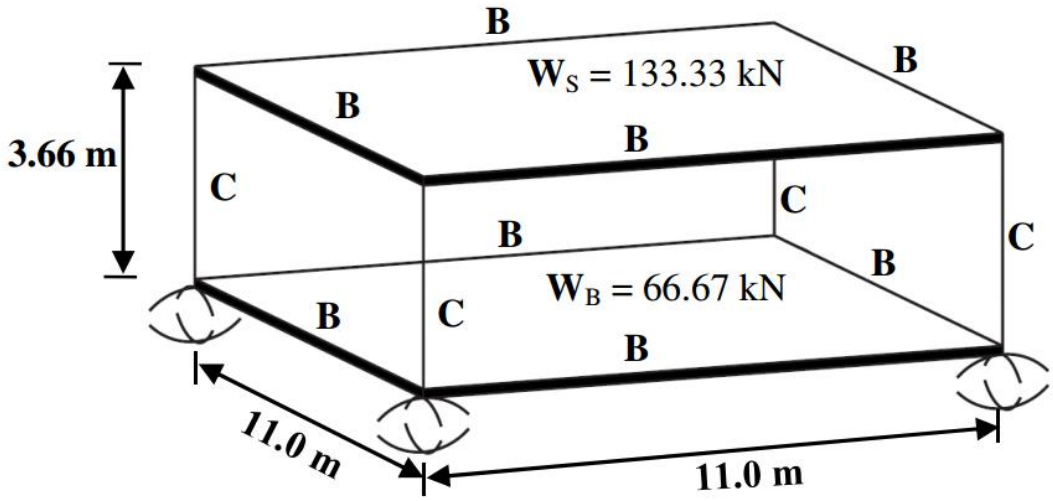

Figure 3. Schematic form of the three-dimensional structure with a single degree of freedom [23]

Table 3: Specifications of the three-dimensional structure with a single degree of freedom [23].

Section Property	Area (mm^2)	Moment of Inertia (mm^4)	Torsion Constant (mm^4)	Shear Area (mm^2)
Column (C)	5.0×10^6	6.851×10^7	1.0×10^8	5.0×10^6
Beam (B)	5.0×10^6	1.0×10^{11}	1.0×10^8	5.0×10^6

Table 4: Specifications of the triple friction pendulum bearing [23].

	R_{eff} (mm)	μ	d (mm)
Surface 1	435	0.04	64
Surfaces 2 & 3	52	0.02	19
Surface 4	435	0.13	64

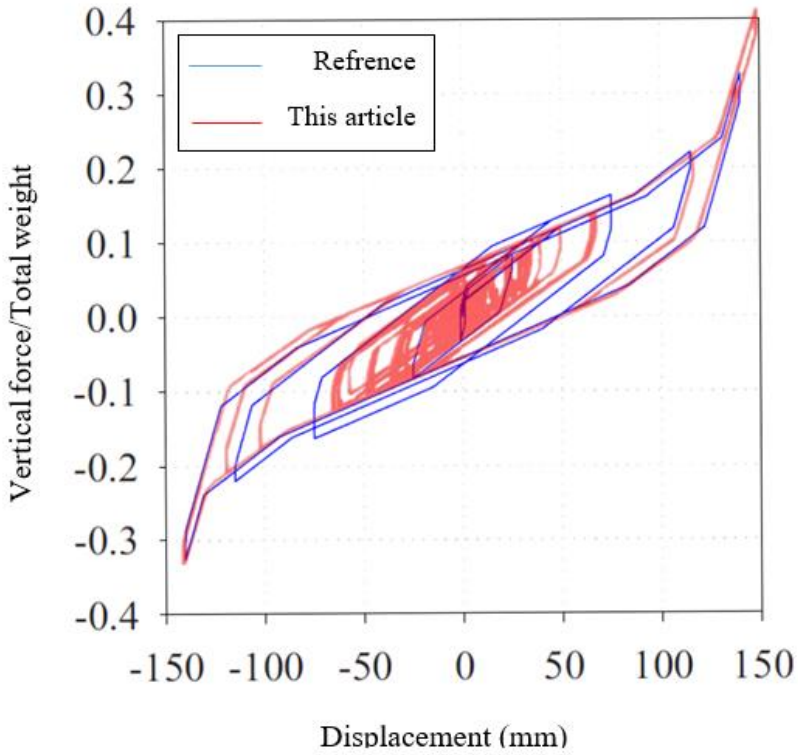

Figure 4. Comparison of the hysteresis diagram of the isolated structure with the reference article [12]

7. SELECTION OF EARTHQUAKES

This paper selects seven pairs of earthquake records to perform the nonlinear time history analysis and IDA of the 4-story structure among the 32 earthquakes introduced in Table 5. These earthquakes are selected based on the total damage criteria computed based on the Park-Ang damage index and Chandler's classification to have the maximum total damage index and cover all three categories of Chandler's classification (Table 6).

Table 5: 32 main shocks, along with their seismic information.

Earthquake	Significant Duration *(sec)*	Arias Intensity (m/sec)	PGA *(g)*	PGA/PGV *(g.sec/m)*	PADI	Max. Drift Global	Max. Roof Disp. *(m)*	Max. Drift local
Coalinga	8.155	4.127	0.602	0.9950	0.1933	0.152	0.1962	0.0261
Coalinga	9.07	3.827	0.525	1.3392	0.0977	0.0085	0.1093	0.0186
Chalfant valley	12.76	0.504	0.254	1.3879	0.0131	0.0091	0.1171	0.011
Chalfant valley	7.26	1.944	0.444	1.2402	0.1043	0.0116	0.1503	0.0201
Chalfant valley	10.92	0.136	0.168	3.4285	0.005	0.0008	0.0104	0.0011

imperial valley	14.81	0.754	0.203	1.0855	0.007	0.0049	0.0632	0.0066
imperial valley	9	1.999	0.367	1.0194	0.0165	0.0076	0.0982	0.0074
imperial valley	14.15	0.701	0.223	0.5150 1	0.0005	0.0049	0.0631	0.0031
imperial valley	19.52	0.224	0.136	1.2363	0.0002	0.0024	0.031	0.0088
imperial valley	51.41	2.389	0.236	0.8973	0.0063	0.0066	0.0851	0.0086
Livermore	10.56	0.212	0.149	0.6995	0.0028	0.0067	0.0862	0.0019
Livermore	21.08	0.031	0.043	0.86	0.0004	0.0014	0.0186	0.0037
Livermore	7.31	0.214	0.256	1.6623	0.004	0.0084	0.0618	0.0085
Livermore	10.37	0.211	0.15	0.7211	0.0028	0.0067	0.0865	0.0024
Livermore	25.24	0.041	0.055	1.7741	0.0009	0.0018	0.0228	0.0024
Livermore	10.025	0.021	0.045	1.0465	0.0042	0.002	0.0253	0.0018
Livermore	10.335	0.037	0.057	2.111	0.005	0.0014	0.0185	0.0047
mammoth lake	10.845	0.739	0.271	1.9496	0.0006	0.0037	0.0482	0.0047
mammoth lake	10.48	0.739	0.271	1.9496	0.0006	0.0037	0.0482	0.0047
mammoth lake	10.845	0.722	0.271	1.9496	0.0006	0.0037	0.0482	0.0162
Northridge	9.08	2.788	0.568	1.100	0.0884	0.0095	0.1224	0.0141
Northridge	16.12	0.774	0.139	0.691	0.0424	0.0096	0.1237	0.0062
Northridge	14.6	0.329	0.126	0.9767	0.0034	0.0034	0.0438	0.0052
Northridge	11.67	0.244	0.109	1.211	0.0038	0.0041	0.053	0.0059
Northridge	15.45	0.092	0.06	1.0909	0.0039	0.0042	0.0541	0.0097
Northridge	11.86	1.051	0.316	2.257	0.0014	0.0043	0.0549	0.0066
Northridge	12.26	0.538	0.214	1.9814	0.0067	0.0039	0.0505	0.0015
Cape Mendocino	16.26	0.588	0.226	3.183	0.0042	0.0005	0.0027	0.0015
Cape Mendocino	16.1	3.829	0.662	0.7298	0.345	0.0237	0.3047	0.0327
Cape Mendocino	24.6	0.337	0.178	0.631	0.0367	0.0095	0.1222	0.0125
Wittier Narrows	12.38	0.233	0.155	1.220	0.0026	0.0047	0.0608	0.0064
Wittier Narrows	9.755	0.143	0.123	2.6739	0.0045	0.0013	0.0168	0.0066

Table 6: Characteristics of the main earthquakes used in incremental dynamic analysis.

Earthquake	Significant duration *(sec)*	Areas intensity *(m/sec)*	PGA *(g)*	PGV *(m/sec)*	PGA/PGV *(g.sec/m)*	Housner intensity *(m)*	PADI
Coalinga	*8.155*	4.12	0.602	0.605	0.995	4.887	0.1933
Chalfant Valley	7.26	1.497	0.444	0.358	1.240	1.497	0.1043
Imperial Valley	9	1.387	0.367	0.36	1.019	1.387	0.0165
Livermore	7.31	0.589	0.256	0.154	1.662	0.589	0.004
Northridge	16.21	0.818	0.139	0.201	0.6915	0.818	0.0424
Cape Mendocino	16.1	2.874	0.662	0.907	0.7298	2.874	0.345
Wittier Narrows	12.38	0.411	0.155	0.127	1.2204	0.411	0.0026

7.1. Optimization

The main shock earthquake calculates the maximum possible acceleration that the uncontrolled structure can withstand for each earthquake. In this paper, the limitations that are considered for this analysis are the maximum story drift reaching 0.025 (ASCE 7-16) and the failure index of stories reaching 0.4 [29]; if each of these conditions happens, the analysis is stopped, and the corresponding maximum acceleration is considered in the final stage of the analysis. Table 7 shows the results of these analyses. Finally, the optimal parameters for the TFPB are calculated for structures with and without an isolator using the MOCS. The parameters optimized in this algorithm are the friction coefficients between the surfaces and the effective radii of each surface. Optimization operation is performed under a series of restrictions (Eqs. 6-10).

Table 7: The maximum acceleration coefficient of the main shock.

Earthquake	Coalinga	Chalfant Valley	Imperial Valley	Livermore	Northridge	Cape Mendocino	Wittier Narrows
Max. Factor of PGA	0.7	1.0	0.7	0.9	0.4	0.6	0.65

It is worth mentioning that the values of parameters d_1=d_4=0.050 and d_2=d_3=0.010 meters. Table 8 lists the specifications of these separators.

Table 8: Characteristics of TFPB optimized for each earthquake.

Earthquake	μ_1	$\mu_2 = \mu_3$	μ_4	$R_{eff\ 1\&4}$	$R_{eff\ 2\&3}$
Coalinga	0.04	0.02	0.10	0.435	0.052
Chalfant Valley	0.041	0.025	0.129	0.500	0.056
Imperial Valley	0.05	0.02	0.10	0.400	0.050
Livermore	0.06	0.01	0.012	0.620	0.080
Northridge	0.04	0.025	0.10	0.430	0.050
Cape Mendocino	0.03	0.01	0.06	0.350	0.040
Wittier Narrows	0.04	0.02	0.11	0.450	0.045

Based on the optimal values calculated in Table 8, the periodicity of each regime of designed and optimized isolators for each earthquake is calculated using Eqs. (1–3) and presented in Table 9.

Table 9: Periodicity of each regime of designed and optimized isolators for each earthquake.

TFPBs	Regime 1	Regime 2	Regime 3	Regime 4	Regime 5
Coalinga	0.457	1.121	1.432	1.423	1.214
Chalfant Valley	0.4191	1.257	1.337	1.400	1.260
Imperial Valley	0.491	1.012	1.401	1.389	1.182
Livermoor	0.732	1.294	1.470	1.535	1.495
Northridge	0.388	1.103	1.422	1.413	1.188
Cape mendocino	0.327	1.081	1.329	1.305	1.080
Wittier Narrows	0.425	1.154	1.397	1.401	1.168

7.2. Sequence IDA

In this part, the structure controlled by the TFPB is subjected to IDA sequence analysis. First, the main earthquake with the acceleration at which the structure without the isolator had reached its critical limits (Table 7) is applied to the structure with the isolator. Then the structure oscillates for four times of its original period freely. Afterward, the aftershock is applied to the structure on different scales in the next stages. In each stage, this acceleration increases until the maximum story drift reaches 0.025 or the Park-Ang damage index exceeds 0.4. The graphs related to these analyses are presented in Figs. 5–6. Furthermore, the structure with and without isolators are analyzed by IDA again under the main shock and aftershock, and the corresponding graphs are presented.

Fig. 5 shows the maximum value of the intensity factor of the main earthquake when the damage index of the uncontrolled structure reaches 0.4 (the maximum value of the repairable range). As shown in Fig. 5, the non-isolated structure has been subjected to IDA analysis under the effect of main and aftershock earthquakes. It has been subjected to sequence analysis simultaneously. The analysis results for each earthquake are placed separately in each diagram, which is needed for comparison with the isolated structure.

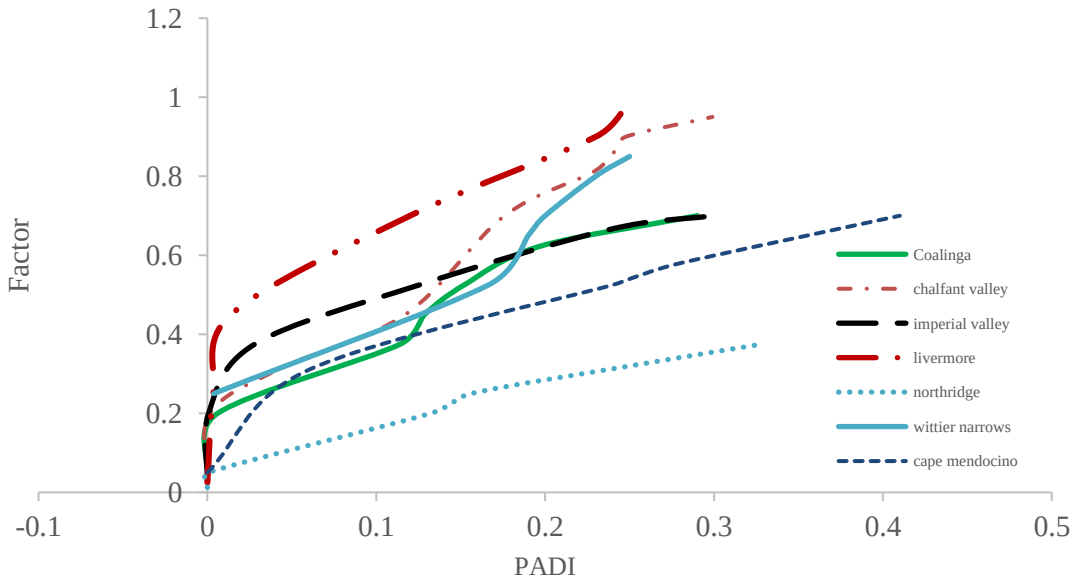

Figure 5: Main shock earthquake intensity chart according to the Park-Ang damage index in the non-isolated structure

The comparison of the graphs in Figs. 6 and 7 shows that the isolated structure reaches the upper limit of layer drift at higher intensities of *1g* than the non-isolated structure. This result is clear in both the IDA analysis under main shock-aftershock earthquakes and the sequence analysis in the graph of each earthquake.

The results obtained from Figs. 5-8 have been compared in Table 10.

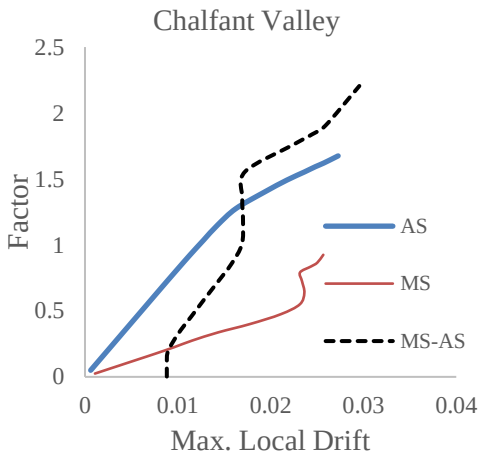
Chalfant Valley
Factor
Max. Local Drift
AS
MS
MS-AS
0
0.5
1
1.5
2
2.5
0.01
0.02
0.03
0.04

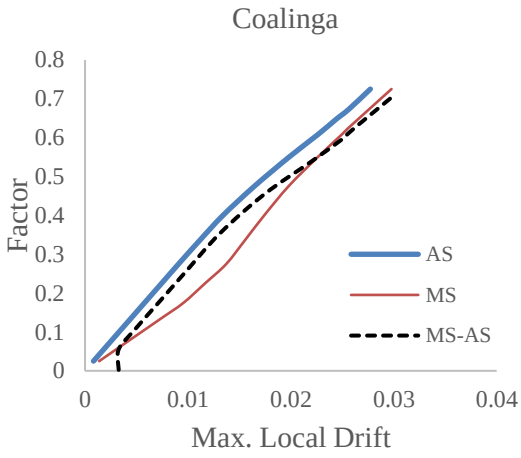
Coalinga
Factor
Max. Local Drift
AS
MS
MS-AS
0
0.1
0.2
0.3
0.4
0.5
0.6
0.7
0.8
0.01
0.02
0.03
0.04

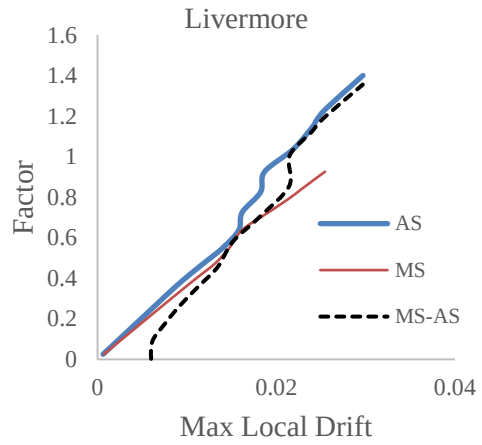
Livermore
Factor
Max Local Drift
AS
MS
MS-AS
0
0.2
0.4
0.6
0.8
1
1.2
1.4
1.6
0.02
0.04

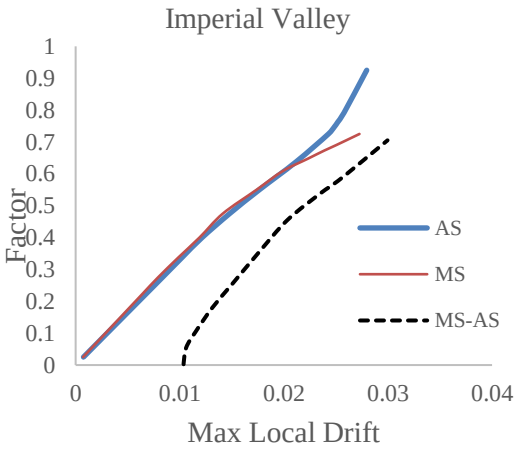
Imperial Valley
Factor
Max Local Drift
AS
MS
MS-AS
0
0.1
0.2
0.3
0.4
0.5
0.6
0.7
0.8
0.9
1
0.01
0.02
0.03
0.04

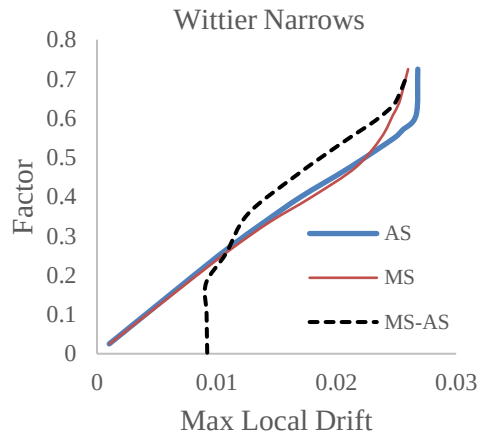
Wittier Narrows
Factor
Max Local Drift
AS
MS
MS-AS
0
0.1
0.2
0.3
0.4
0.5
0.6
0.7
0.8
0.01
0.02
0.03

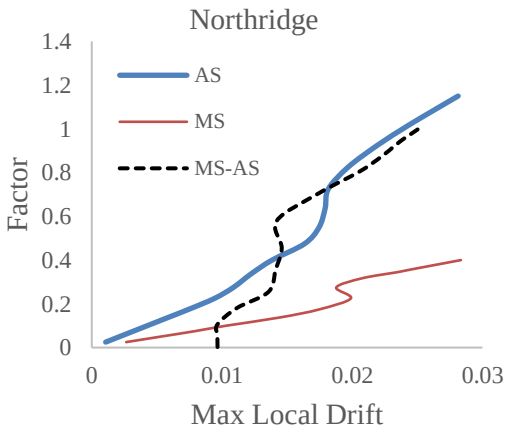
Northridge
Factor
Max Local Drift
AS
MS
MS-AS
0
0.2
0.4
0.6
0.8
1
1.2
1.4
0.01
0.02
0.03

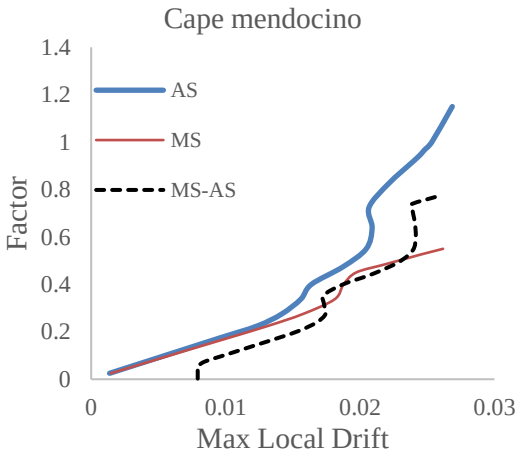

Figure 6: IDA and sequence diagrams for the isolated structure under selected earthquakes

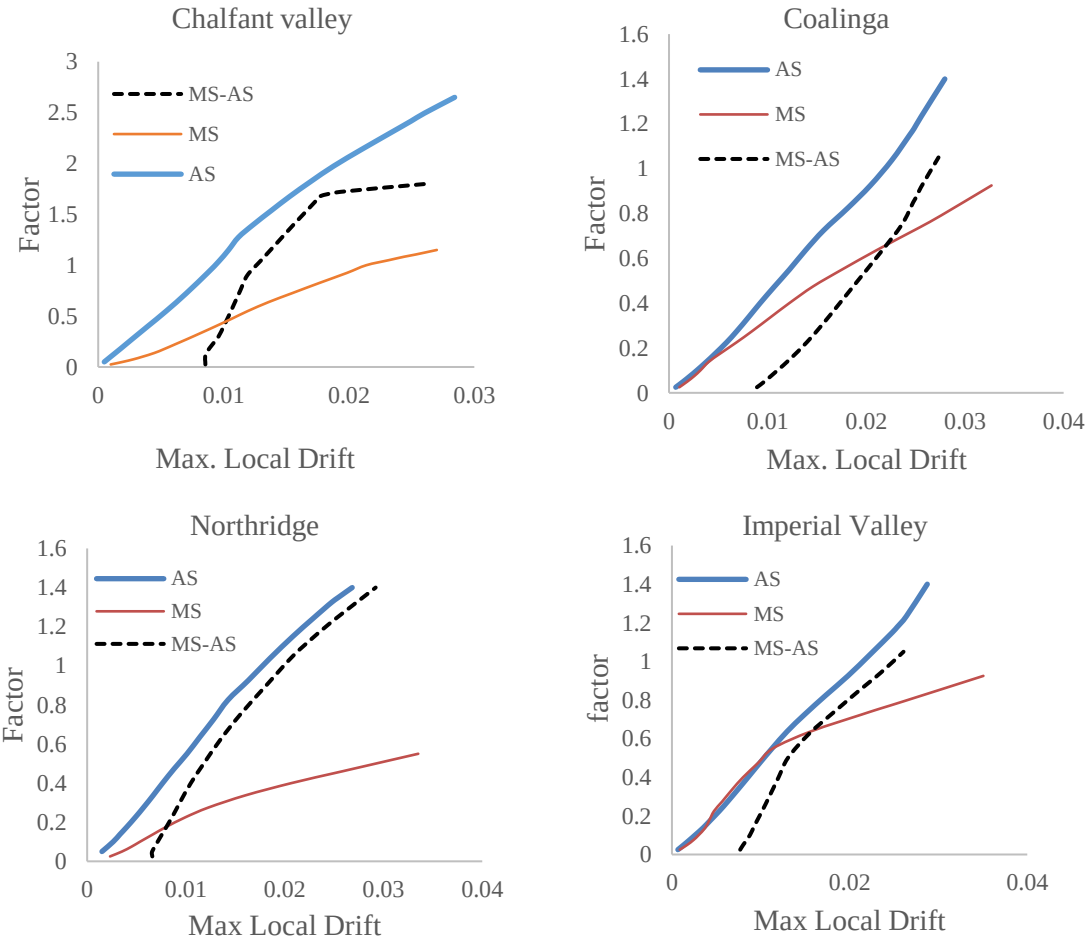

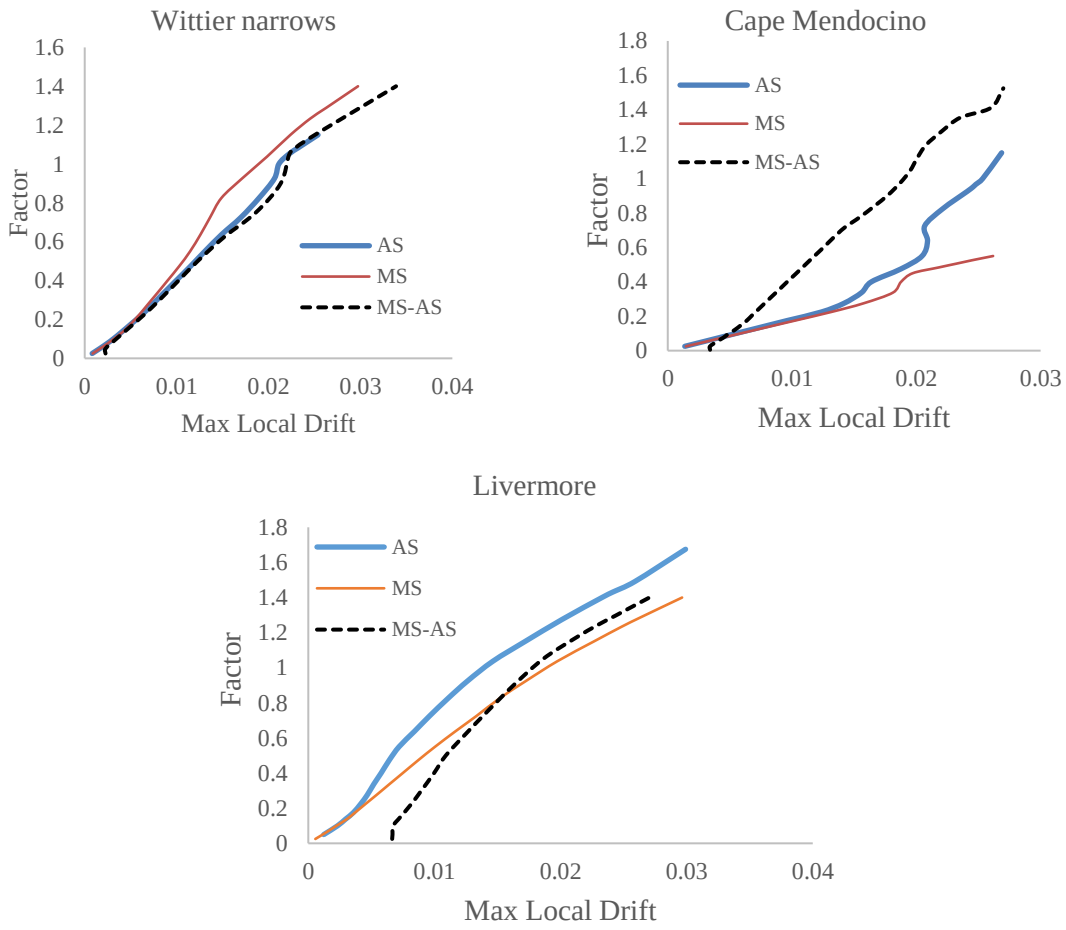

Figure 7: IDA and sequence charts for the isolated structure under selected earthquakes

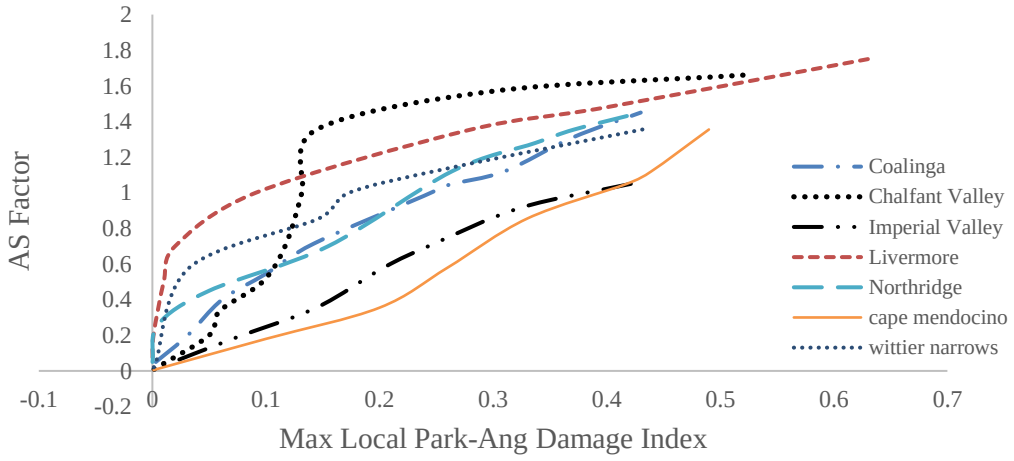

Figure 8: Diagram of sequence analysis results for the isolated structure

Table 10: Results of IDA and sequence analyses performed with selected earthquakes.

Earthquake		Controlled structure			Uncontrolled structure			Rate of
		Fac.	drift	PADI	Fac.	Drift	PADI	change (%)
Coalinga	Ms	0.9	0.025	0.3	0.7	0.035	0.4	28
	As	1.4	0.025	0.36	0.8	0.035	0.4	50
	Ms-As	1	0.025	0.38	0.65	0.025	0.3	53
Chalfant Valley	Ms	2.1	0.025	0.3	1	0.025	0.4	110
	As	2.6	0.025	0.38	1.5	0.025	0.3	73
	Ms-As	1.8	0.025	0.32	1.7	0.025	0.35	5
Livermore	Ms	1.4	0.025	0.29	0.9	0.025	0.4	55
	As	1.6	0.025	0.32	1.2	0.025	0.32	33
	Ms-As	1.4	0.025	0.4	1.2	0.025	0.35	16
Imperial Valley	Ms	0.8	0.025	0.31	0.7	0.03	0.4	100
	As	1.2	0.025	0.3	0.8	0.025	0.33	50
	Ms-As	1	0.025	0.36	0.6	0.025	0.36	66
Cape Mendocino	Ms	0.75	0.025	0.28	0.6	0.025	0.4	87.5
	As	1.15	0.025	0.32	1	0.025	0.38	15
	Ms-As	1.4	0.025	0.41	0.8	0.025	0.36	75
Northridge	Ms	0.45	0.025	0.25	0.36	0.025	0.4	25
	As	1.4	0.025	0.38	1.1	0.025	0.37	27
	Ms-As	1.3	0.025	0.41	1	0.025	0.35	30
Wittier Narrows	Ms	1.2	0.025	0.38	0.65	0.025	0.4	85
	As	1.1	0.025	0.37	0.6	0.025	0.35	83
	Ms-As	1.1	0.025	0.39	0.7	0.025	0.3	57

It can be found from the comparison of the graphs in Figs. 5-8 that the structure equipped with an isolator has a much better seismic performance than the non-isolated structure in different earthquakes. The maximum tolerable acceleration improved by 5% to 75% compared to the unseparated state.

8. CONCLUSION

After analyzing the graphs and data output from the analysis. The following results are obtained:

1. The IDA analysis of the structure without isolators and isolators provides this platform to check the performance of the structure and isolators under the effect of earthquakes that are not followed by aftershocks. Therefore, by comparing the IDA diagrams of structures, the effect of the existence of the optimized isolator in improving the structure's performance can be compared.
2. In all three analysis modes, the damage index in an isolated structure reaches higher earthquake intensities, indicating an improvement of at least 5% (in the Chalfant Valley earthquake) and at most 75% (for the Cape Mendocino earthquake) in the structure's performance.

3. The second criterion of the analysis, which is the maximum class drift, reaches the critical value of 0.025 in the isolated structure at higher earthquake intensities in all three analyses of the main shock-aftershock and sequence.
4. The structure with the isolator, after it is damaged at the maximum intensity, continues with greater intensities of the AfterShock earthquake before meeting the critical value of the Park-Ang damage index. This indicates a good improvement in the performance of the optimized isolators for each earthquake.

9. ACKNOWLEDGMENTS

The authors would like to show their appreciation to the HPC center (Shahr-e-Kord University, Iran) for their collaboration in offering computational clusters, which was a great help in completing this work.

REFERENCE

1. Mazloom M. Studying the Park-Ang damage index of reinforced concrete structures based on equivalent sinusoidal waves. *Struct Eng Mech*. 2019;**72**(1):83-97.
2. Hait P, Sil A, Choudhury S. Seismic damage assessment and prediction using artificial neural network of RC building considering irregularities. *J Struct Integr Maint*. 2020;**5**(1):51-69.
3. Park YJ, Ang AH. Mechanistic seismic damage model for reinforced concrete. *J Struct Eng*. 1985;**111**(4):722-39.
4. Ghobarah A, Abou-Elfath H, Biddah A. Response-based damage assessment of structures. *Earthq Eng Struct Dyn*. 1999;**28**(1):79-104.
5. Gol AA, Bakhshi A, Tabeshpour M. Vulnerability and damage analysis of existing buildings; 2005.
6. Estekanchi H, Arjomandi K, Vafai A. Estimating structural damage of steel moment frames by endurance time method. *J Constr Steel Res*. 2008;**64**(2):145-55.
7. Khaaloo A, Omidi H. A new lateral load pattern for optimum design of concrete structures using the wave propagation theory. *Struct*. 2022.
8. Behnamfar F, Hosseini-Rad A, Habiby YM. A procedure for damage-based seismic design of moment frame structures; 2021.
9. Zayas VA, Mahin SA. The FPS earthquake resisting system experimental report. *Earthq Eng Res Center*. 1987.
10. Fenz DM, Constantinou MC. Behaviour of the double concave friction pendulum bearing. *Earthq Eng Struct Dyn*. 2006;**35**(11):1403-24.
11. Mokha A, Constantinou M, Reinhorn A. Teflon bearings in base isolation I: testing. *J Struct Eng*. 1990;**116**(2):438-54.

12. Fenz DM, Constantinou MC. Modeling triple friction pendulum bearings for response-history analysis. *Earthq Spectra*. 2008;**24**(4):1011-28.
13. Fenz DM, Constantinou MC. Spherical sliding isolation bearings with adaptive behavior: Experimental verification. *Earthq Eng Struct Dyn*. 2008;**37**(2):185-205.
14. Keikha H, Ghodrati Amiri G. Seismic performance assessment of quintuple friction pendulum isolator with a focus on frictional behavior impressionability from velocity and temperature. *J Earthq Eng*. 2019;1-31.
15. Kaveh A, Biabani Hamedani K. A hybridization of growth optimizer and improved arithmetic optimization algorithm and its application to discrete structural optimization. *Comput Struct*. 2024;**303**:107496.
16. Kaveh A, Eskandari A. Tuned African vultures optimization algorithm for optimal design of skeletal structures employing multi-stage parameter adjustment. *Iran J Sci Technol Trans Civ Eng*. 2025;**49**(2):1211-32.
17. Etedali S, Hasankhoie K, Sohrabi MR. Optimal design of pure-friction isolators with and without restoring device: A multi-objective cuckoo search-based approach for seismic-excited structures. *Struct*. 2020.
18. Keikha H, Ghodrati Amiri G. Numerical development and assessment of 3D quintuple friction pendulum isolator element based on its analytical and mathematical models. *J Earthq Eng*. 2019;1-40.
19. Dao ND, Ryan KL, Sato E, Sasaki T. Predicting the displacement of triple pendulum™ bearings in a full-scale shaking experiment using a three-dimensional element. *Earthq Eng Struct Dyn*. 2013;**42**(11):1677-95.
20. Kunnath SK, Reinhorn AM, Lobo R. IDARC Version 3.0: A program for the inelastic damage analysis of reinforced concrete structures. *Natl Cent Earthq Eng Res Buffalo NY*. 1992.
21. Cosenza E, Manfredi G, Ramasco R. The use of damage functionals in earthquake engineering: A comparison between different methods. *Earthq Eng Struct Dyn*. 1993;**22**(10):855-68.
22. Díaz SA, Pujades LG, Barbat AH, Hidalgo-Leiva DA, Vargas-Alzate YF. Capacity, damage, and fragility models for steel buildings: A probabilistic approach. *Bull Earthq Eng*. 2018;**16**(3):1209-43.
23. Amiri GG, Namiranian P, Amiri MS. Seismic response of triple friction pendulum bearing under near-fault ground motions. *Int J Struct Stab Dyn*. 2016;**16**(06):1550021.
24. Maulana TI, Enkhtengis B, Saito T. Proposal of damage index ratio for low-to mid-rise reinforced concrete moment-resisting frame with setback subjected to uniaxial seismic loading. *Appl Sci*. 2021;**11**(15):6754.
25. Yang XS, Deb S. Engineering optimisation by cuckoo search. *arXiv preprint arXiv:1005.2908*. 2010.
26. Rajabioun R. Cuckoo optimization algorithm. *Appl Soft Comput*. 2011;**11**(8):5508-18.

27. Salimi M, Kamgar R, Heidarzadeh H. An evaluation of the advantages of friction TMD over conventional TMD. *Innov Infrastruct Solut*. 2021;**6**(2):95.
28. Ibarra LF, Krawinkler H. Global collapse of frame structures under seismic excitations. *John A Blume Earthq Eng Center*. 2005.
29. Williams MS, Sexsmith RG. Seismic damage indices for concrete structures: A state-of-the-art review. *Earthq Spectra*. 1995;**11**(2):319-49.